Lab 4 Report:

Abstract:

Every sensor measurement inevitably contains errors, commonly manifesting as noise in datasets. Recognizing and understanding this noise is essential when developing systems based on particular sensors and technologies. For our study, we employed the VN-100 Inertial Measurement Unit (IMU) to gather data on stationary angular motion, velocity, acceleration, and magnetic fields. This data was recorded over two distinct intervals: a short span of 15 minutes. By plotting this sequential data and determining Allan Variances, we aimed to interpret the influence of noise on our readings.

Data collection

IMU devices combine gyroscopes, accelerometers, magnetometers, and pressure sensors, enabling them to measure movements across a three-dimensional axis. Their meticulous calibration ensures the accurate detection of minute shifts in motion and orientation. Owing to this sensitivity, the data is susceptible to noise. To mitigate such interference, we opted to gather data at a stationary point. This site was selected due to its distance from train routes, ensuring fewer disturbances, and the basement's natural insulation from external factors like wind and vibrations.

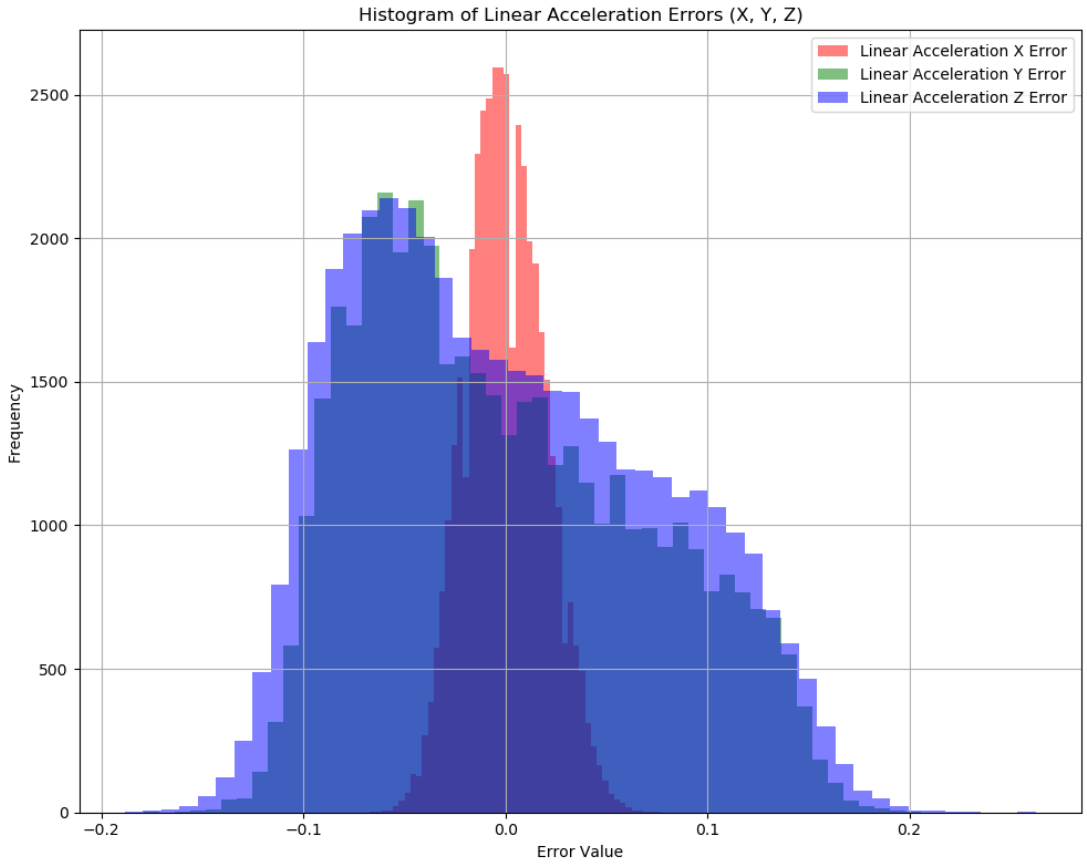

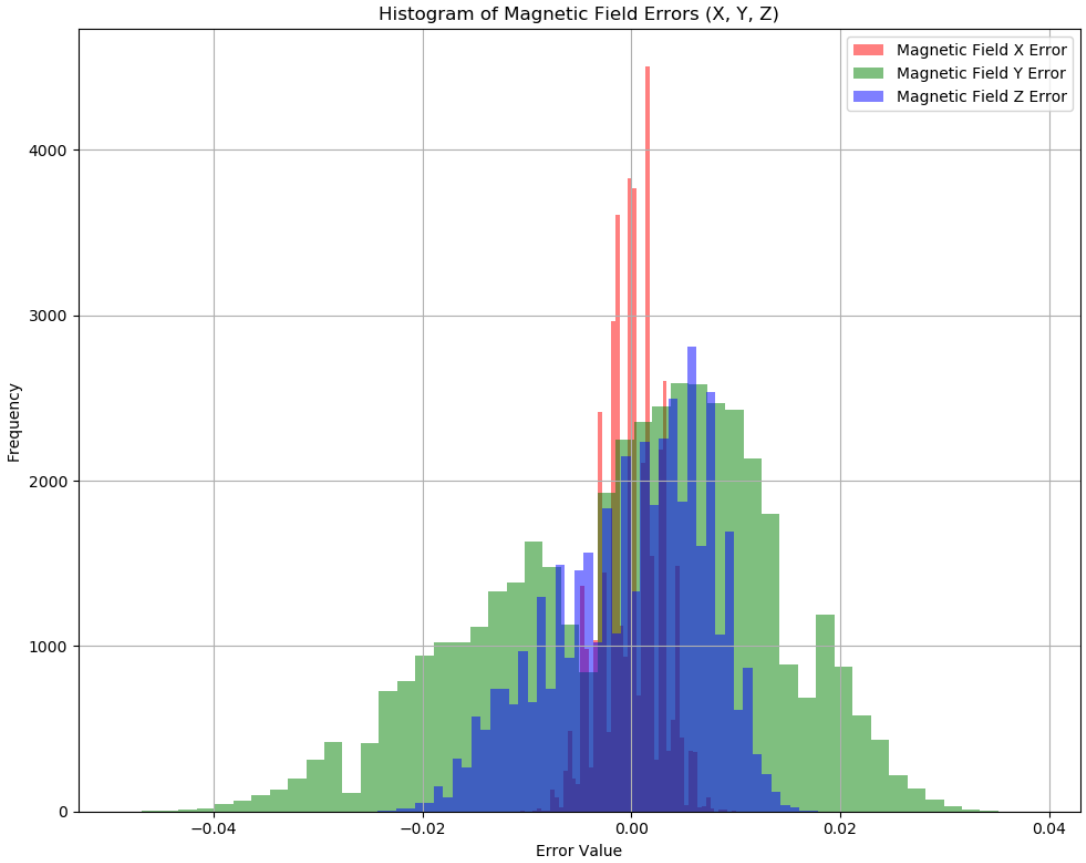
Histogram of Magnetic Field Errors (X, Y, Z)
Magnetic Field X Error
Magnetic Field Y Error
Magnetic Field Z Error
Frequency
Error Value
0
1000
2000
3000
4000
−0.04
−0.02
0.00
0.02
0.04

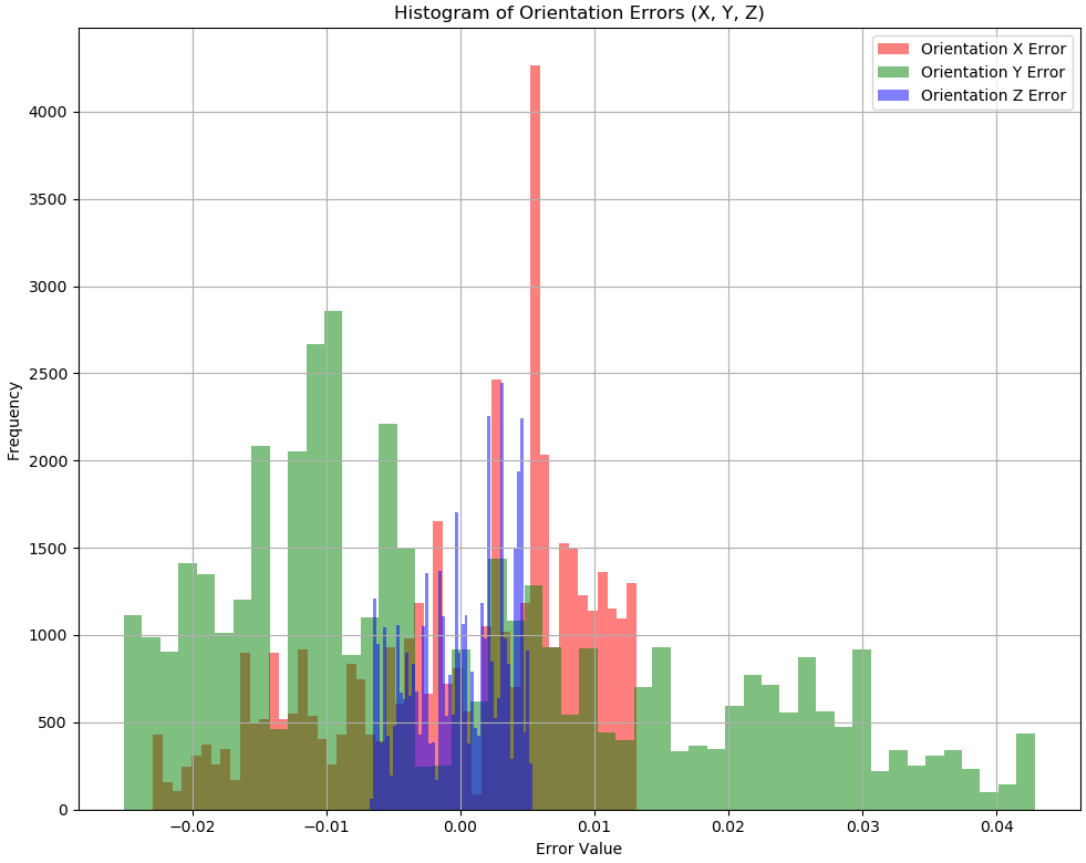
Histogram of Orientation Errors (X, Y, Z)
Orientation X Error
Orientation Y Error
Orientation Z Error
Frequency
Error Value
0
500
1000
1500
2000
2500
3000
3500
4000
−0.02
−0.01
0.00
0.01
0.02
0.03
0.04

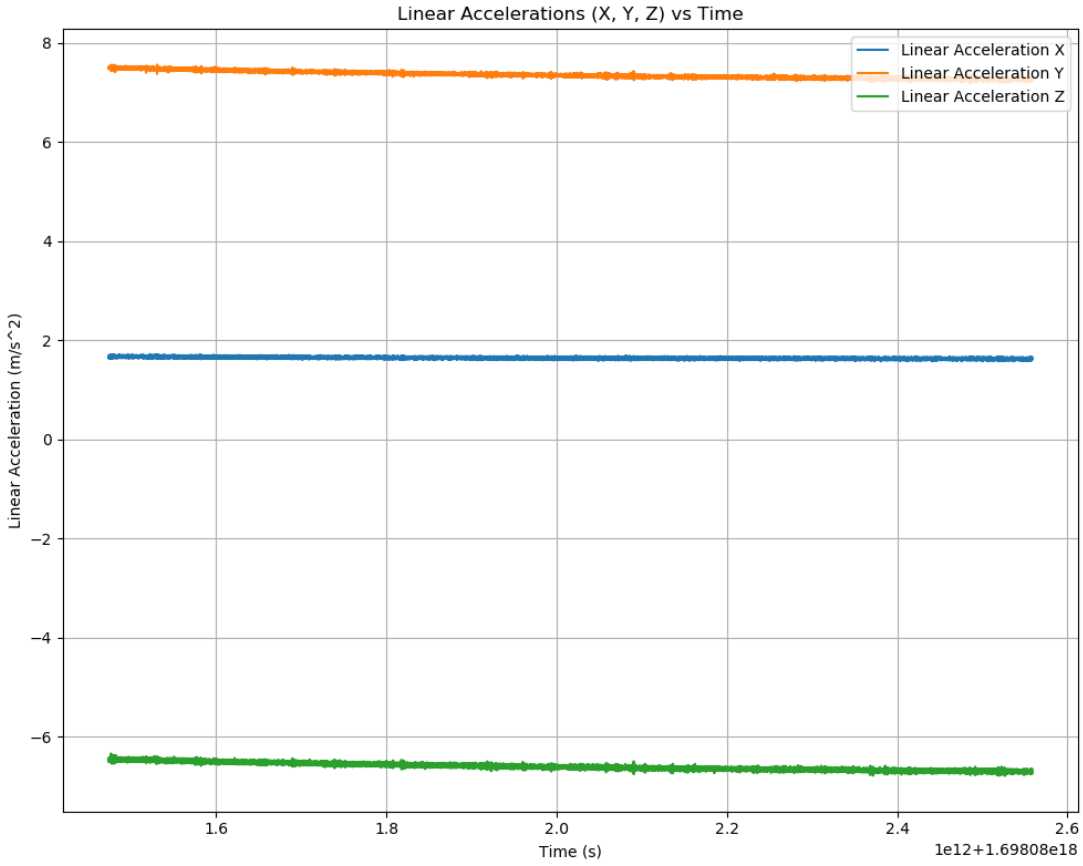
Linear Accelerations (X, Y, Z) vs Time
Linear Acceleration X
Linear Acceleration Y
Linear Acceleration Z
Linear Acceleration (m/s^2)
8
6
4
2
0
−2
−4
−6
1.6
1.8
2.0
2.2
2.4
2.6
Time (s)
1e12+1.69808e18

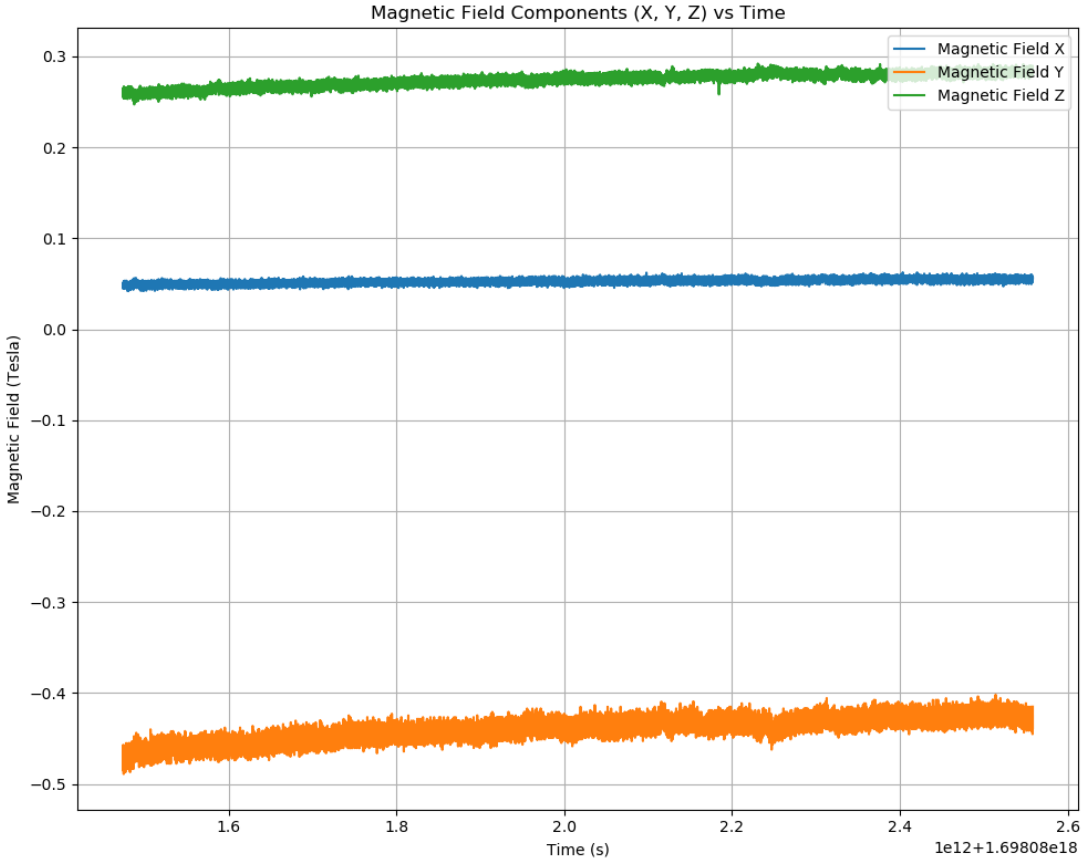
Magnetic Field Components (X, Y, Z) vs Time
Magnetic Field X
Magnetic Field Y
Magnetic Field Z
Magnetic Field (Tesla)
0.3
0.2
0.1
0.0
−0.1
−0.2
−0.3
−0.4
−0.5
1.6
1.8
2.0
2.2
2.4
2.6
Time (s)
1e12+1.69808e18

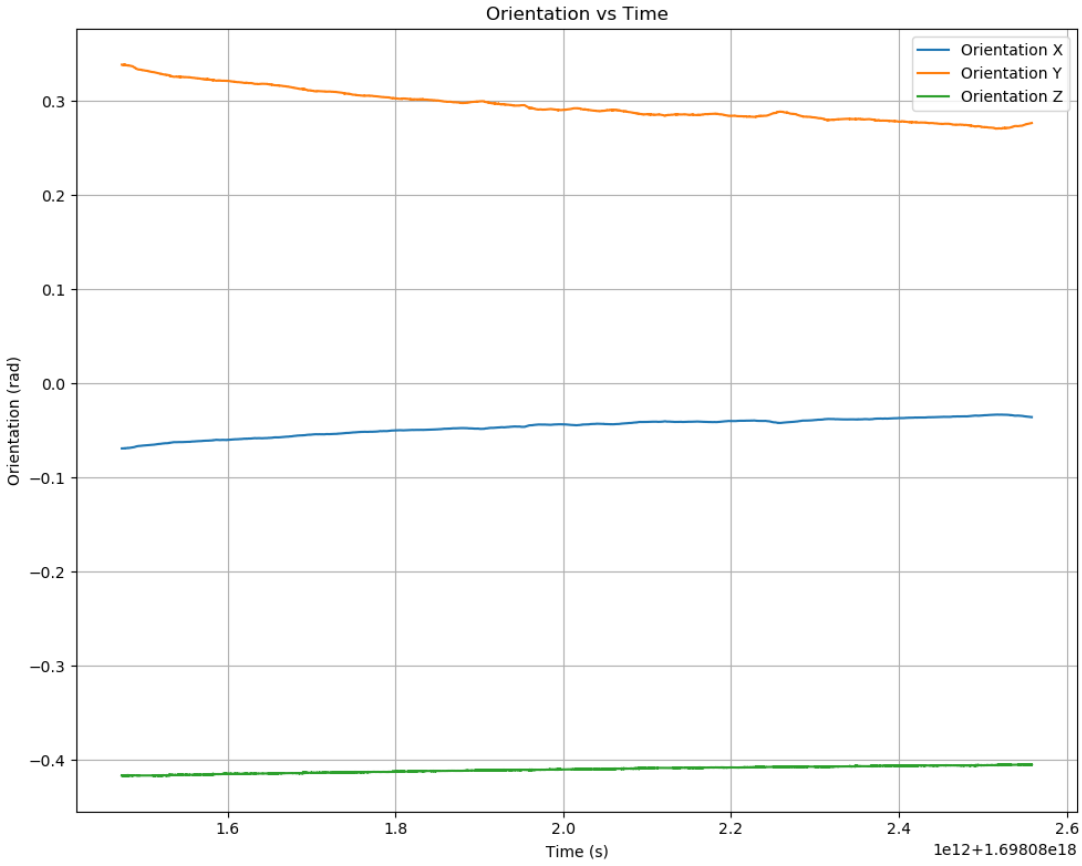
Orientation vs Time
Orientation X
Orientation Y
Orientation Z
Orientation (rad)
0.3
0.2
0.1
0.0
−0.1
−0.2
−0.3
−0.4
1.6
1.8
2.0
2.2
2.4
2.6
Time (s)
1e12+1.69808e18

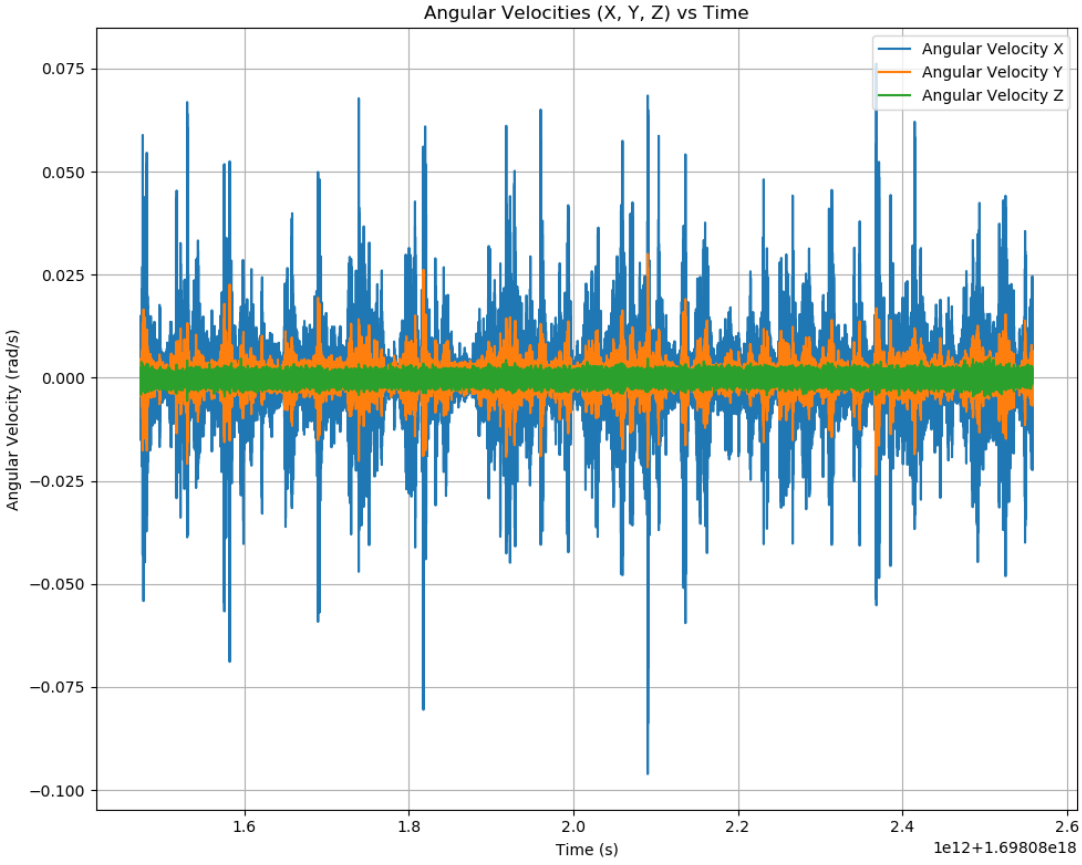
Angular Velocities (X, Y, Z) vs Time
Angular Velocity X
Angular Velocity Y
Angular Velocity Z
Angular Velocity (rad/s)
0.075
0.050
0.025
0.000
−0.025
−0.050
−0.075
−0.100
1.6
1.8
2.0
2.2
2.4
2.6
Time (s)
1e12+1.69808e18

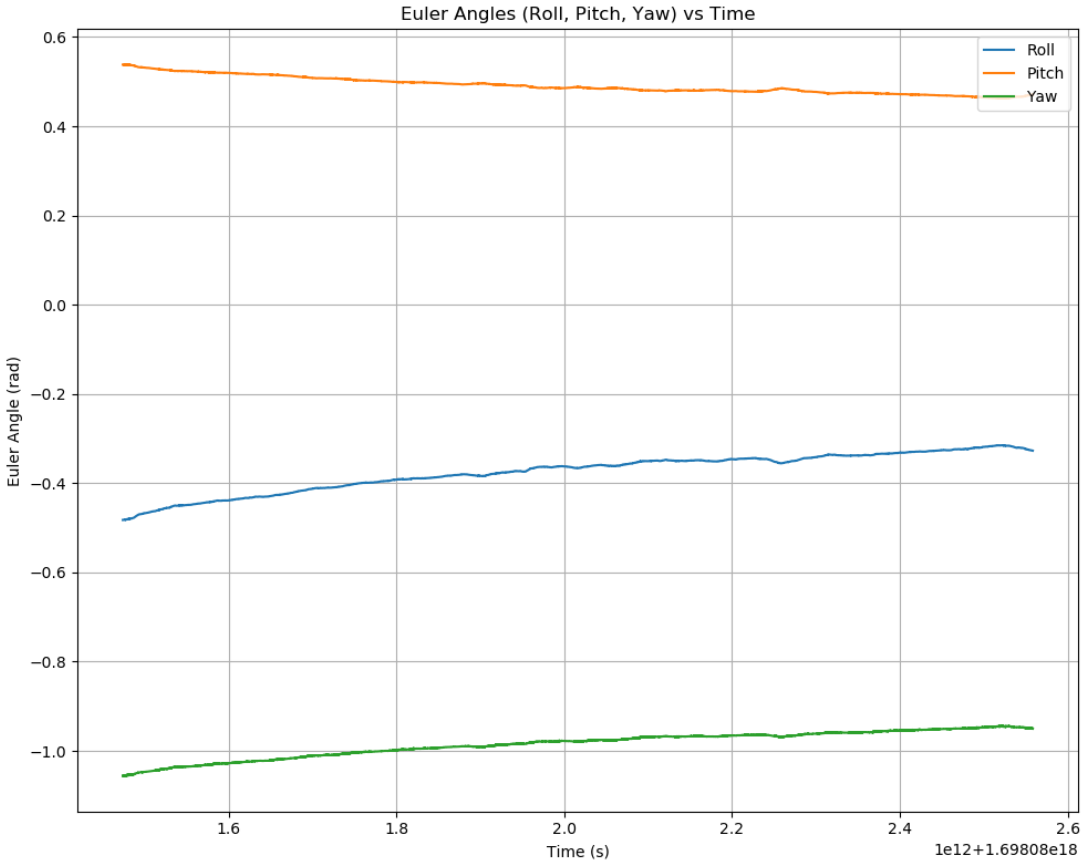
Euler Angles (Roll, Pitch, Yaw) vs Time
Roll
Pitch
Yaw
Euler Angle (rad)
0.6
0.4
0.2
0.0
−0.2
−0.4
−0.6
−0.8
−1.0
1.6
1.8
2.0
2.2
2.4
2.6
Time (s)
1e12+1.69808e18

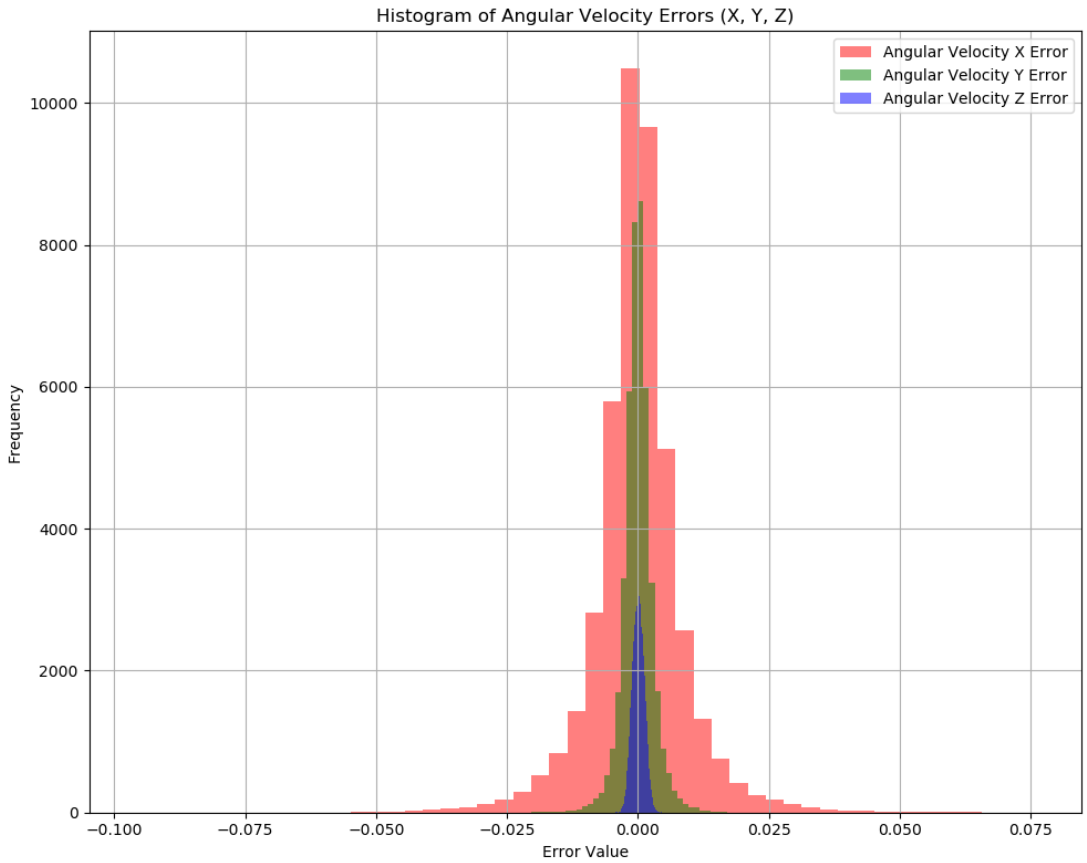
Histogram of Angular Velocity Errors (X, Y, Z)
Angular Velocity X Error
Angular Velocity Y Error
Angular Velocity Z Error
Frequency
10000
8000
6000
4000
2000
0
−0.100
−0.075
−0.050
−0.025
0.000
0.025
0.050
0.075
Error Value

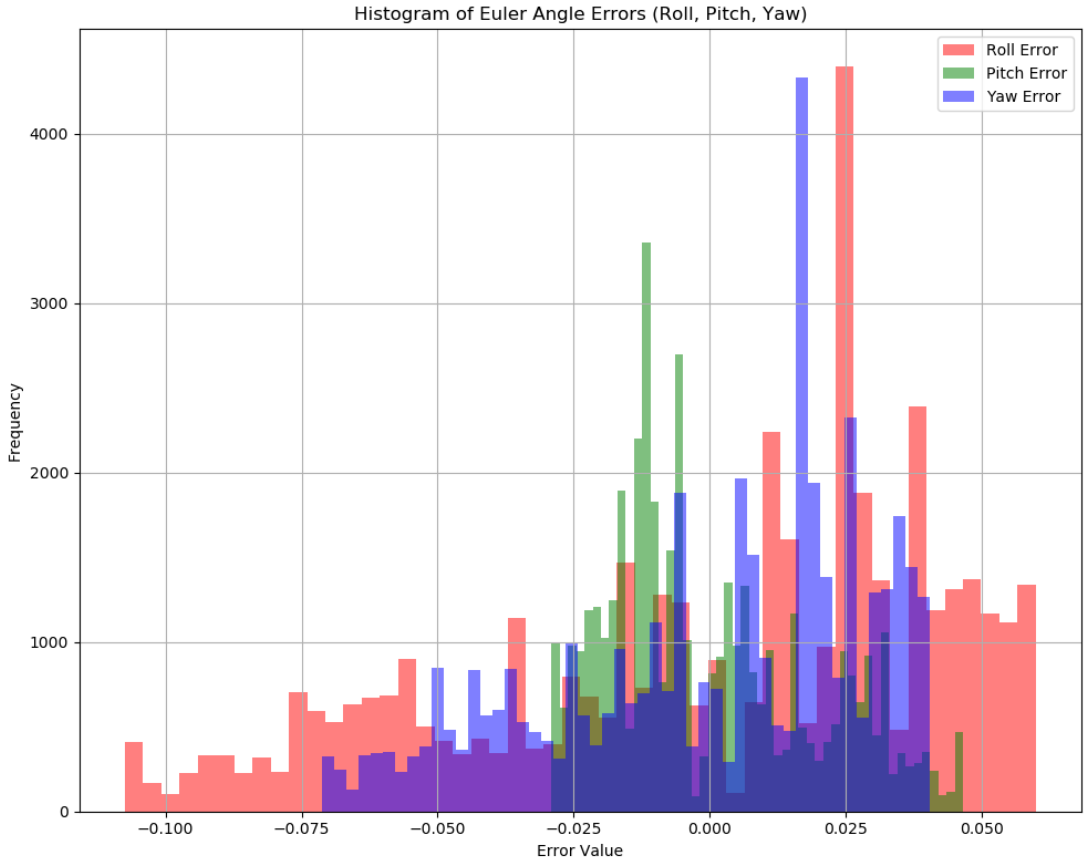

Field	Bias	Error
Angular Velocity X	0.000094	0.008825
Angular Velocity Y	0.000045	0.002883
Angular Velocity Z	-0.000177	0.001151
Magnetic Field X	0.052564	0.002732
Magnetic Field Y	-0.440530	0.013230
Magnetic Field Z	0.274196	0.007273
Linear Acceleration X	1.642171	0.019294
Linear Acceleration Y	7.352119	0.069748
Linear Acceleration Z	-6.598570	0.074202
Orientation X	-0.046080	0.009169
Orientation Y	0.296050	0.017124
Orientation Z	-0.410264	0.003435

Orientation Metrics: Bias Values: The bias values for orientation in X, Y, and Z directions are -0.046080, 0.296050, and -0.410264, respectively. This indicates that the device might not have been perfectly flat, as seen from the non-zero bias values. Error Analysis: The error values show slight variations, with the highest being for the Y orientation at 0.017124. This further points towards the fact that the device was probably lying at a slight angle.

Angular Velocity Metrics: Bias Values: The bias for the angular velocities is close to zero across all axes, specifically X, Y, and Z with values 0.000094, 0.000045, and -0.000177, respectively. This is consistent with the expectation for a stationary device.

Error Analysis: The errors in angular velocity are minimal, with the highest being in the X direction at 0.008825. These values indicate that the device had little to no movement during the measurement.

Magnetic Field Metrics: Bias Values: The magnetic field in the X, Y, and Z directions shows bias values of 0.052564, -0.440530, and 0.274196, respectively. This indicates there might have been some magnetic interference, although the device had no magnetic sources near it. Error Analysis: The errors in the magnetic field, especially in the Y direction (-0.440530 with an error of 0.013230), suggest potential influences or calibrations issues with the magnetometer.

Linear Acceleration Metrics: Gravity Observation: The Z direction shows a linear acceleration of -6.598570 m/s^2, which is close to the gravitational pull of -9.81 m/s^2. The discrepancy could be due to calibration issues or other influencing factors. Bias in X and Y Directions: The linear acceleration in X and Y directions are 1.642171 m/s^2 and 7.352119 m/s^2, which indicates a certain tilt or orientation of the device. Error Analysis: The error values are slightly larger in the linear acceleration data compared to other metrics, suggesting potential disturbances or influences during data capture.

Most standard deviations (errors) are an order of magnitude smaller than their corresponding mean values, demonstrating consistent measurements with low variance. The variations observed in the metrics are attributed to natural errors, such as slight tilts in the device's orientation, calibration issues, or external influences. Within a 15-minute dataset span, it's evident that the Angular Velocity, Linear Acceleration, and Magnetic Flux closely follow a normal distribution. Nevertheless, any noticeable differences from this normal distribution could be attributed to the data being separated into three distinct axes or potentially due to external interferences. This is especially evident in the angular velocity and magnetic histograms. In contrast, only portions of the other two datasets seem to fit a normal distribution. Such discrepancies might arise from unexpected disturbances such as vibrations from nearby trains or inherent traits of the building's structure.

The Orientation and Linear data deviate significantly from a perfect zero bias, indicating potential drifts or inherent biases. On the other hand, the Magnetic data's bias isn't centered around zero, possibly resulting from external magnetic influences or intrinsic sensor biases.
Discussing the data conversion, the datasets were converted into quaternions. To guarantee the precision of this transformation, inverse transformation methodologies were applied. Comparing the original Euler angles with the converted ones and observing the congruent shapes in scatter plots for orientation and Euler angles solidifies our confidence in maintaining data integrity throughout these processes.

Part two:

Abstract

This study focuses on addressing positioning challenges in transient environments using various devices. We employed the VN-100 Inertial Measurement Unit (IMU) to gather data from an accelerometer, gyroscope, and magnetometer, and the GPS Receiver for positioning details. After processing the collected data, we compared the devices' trajectories during a drive around Boston, thereby assessing their precision in recording positioning data.

Data Collection

Our experiment involved driving and obtaining data from both the IMU and GPS. Proper device placement was crucial. The IMU was strategically positioned on the car's dashboard at a flat angle, ensuring its x-axis aligned straight ahead. This arrangement was based on the assumption of operating in a 2D plane with the x-axis denoting the car's direction. The GPS was set atop the IMU, aligned to maximize its communication with surrounding satellites and optimize data accuracy.

Yaw angles and heading

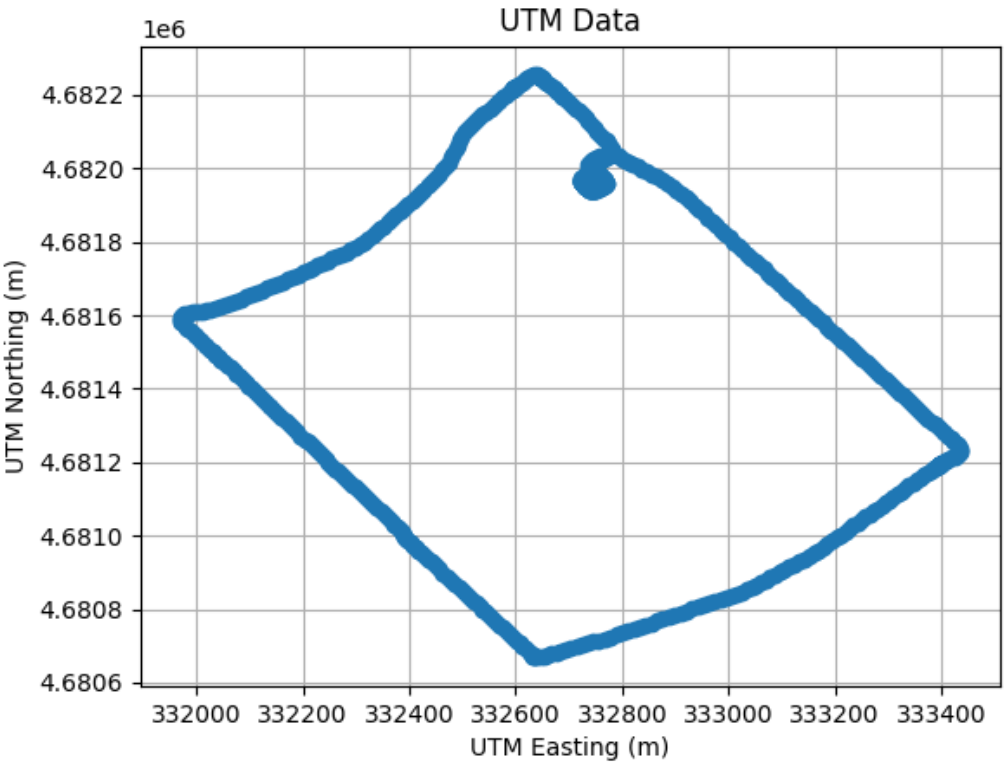

Figure 1

In figure 1, there is one graph for the gps UTM northing vs UTM easting. It states that the

path we drive which is circle for several times and then do a loop. It set up the base for this lab.

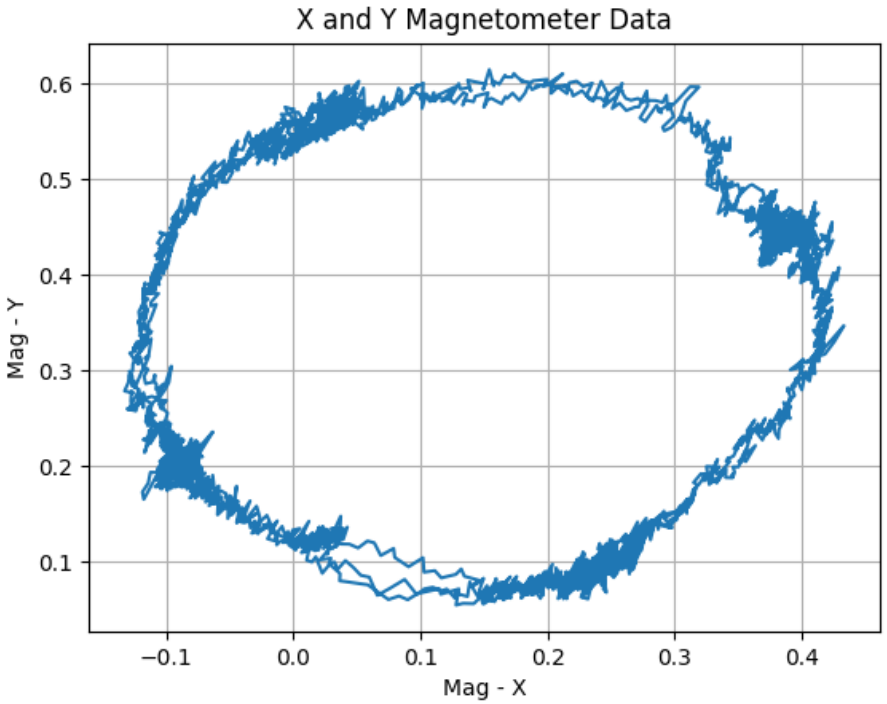

Figure 2

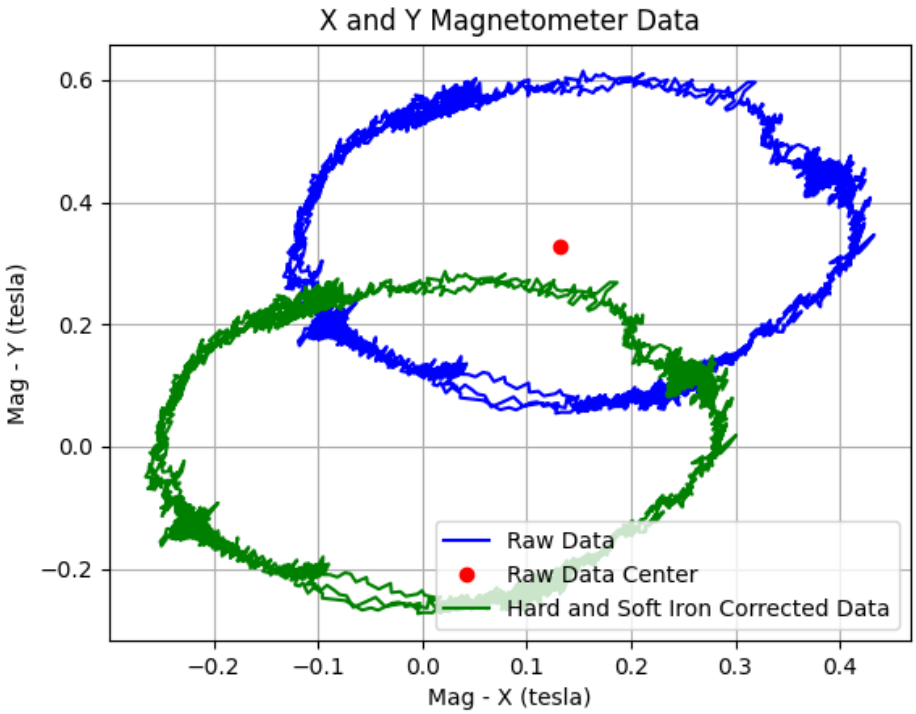

Figure 3

Then there is another graph for the circular circle path as shown in Figure 2, But it obviously not in the center of the graph, so adding the corrections will be the next step. I adjusted the vehicle's heading or yaw angle by considering the hard-iron and soft-iron discrepancies in the magnetometer readings. Hard-iron discrepancies arise from magnetic field changes linked to the sensor's position, manifesting as a consistent bias in the magnetometer readings. On the other hand, soft-iron distortions result in the stretching or warping of the magnetic field. Both these distortions can be visualized and rectified by charting the magnetometer data. The unprocessed magnetometer readings, combined with the data corrected for hard-iron and soft-iron distortions, are presented in figure 3. Using the corrected magnetometer data, I will be able calculate an estimated yaw angle for each Magnetic Field X and Y set using the following equation:

$$yaw = arctan2(M_x / M_y) \qquad \text{(Eq. 1)}$$

I determined an additional yaw estimate by integrating the Z-axis angular velocity from the IMU device. Integrating the angular velocity provides the angle, with the Z-axis rotation indicating the yaw angle, given the orientation of our IMU during data gathering. I then used a complementary filter on both yaw estimates using the subsequent formula:

$$filter = 0.9 * (integrated\ yaw) + 0.1 * (magnetometer\ yaw) \qquad \text{(Eq. 2)}$$

Plots of all yaw calculations are seen below:

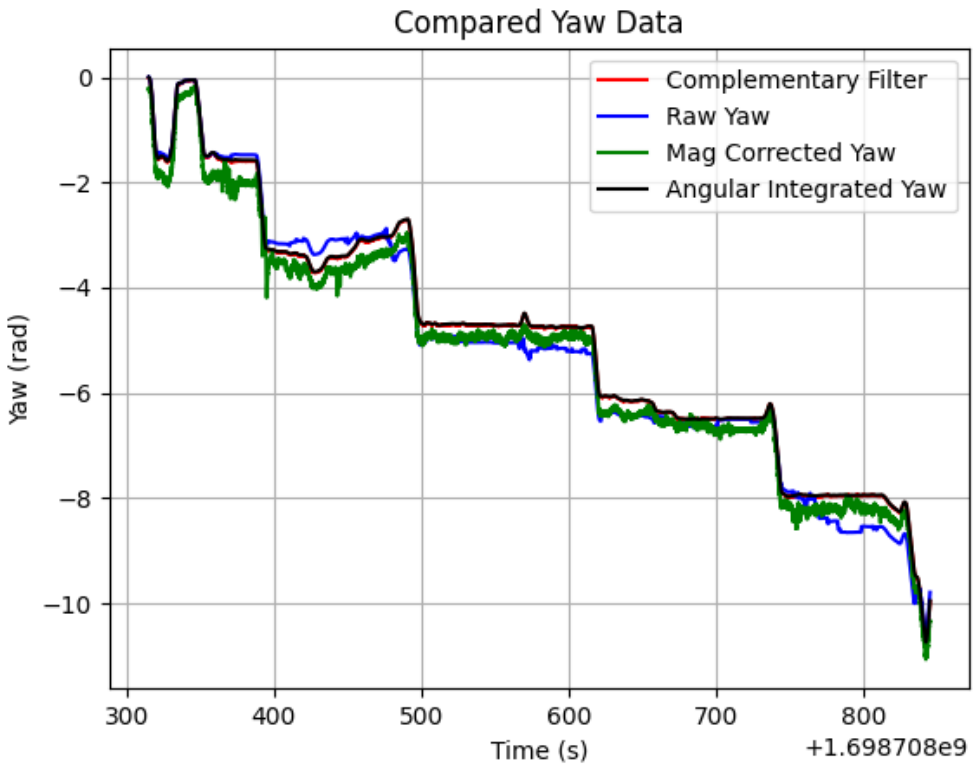

Figure 4

Complementary Filter: The complementary filter evidently offers a smoother and more consistent portrayal of the yaw angle. Its role is to combine the short-term accuracy of one metric (typically the gyroscope) with the long-term stability of another (like an accelerometer or magnetometer).

Raw Yaw: This displays the direct, unrefined yaw data from the sensor. As anticipated, it's more prone to noise and variations, leading to its wavering appearance.

Mag Corrected Yaw: After applying magnetic adjustments to the raw yaw data, there's noticeable stabilization. However, it isn't entirely in sync with the complementary filter.

Angular Integrated Yaw: This curve reflects the yaw angle derived from integrating angular velocities. Due to the nature of integration, errors can pile up over time, causing drifts, which seems evident here.

It's significant to note that the Complementary Filter remains steadfast across both visual representations, highlighting its effectiveness in blending data sources for a robust yaw depiction. While the introduction of IMU angle data in the initial graph adds another layer, the roles of magnetic correction and the complementary filter are essential for a more precise yaw interpretation.

From Figure 4, we can infer that the yaw from the adjusted magnetometer data has more fluctuations compared to the integrated angular rate. Such irregularities arise mainly from the magnetometer's susceptibility to external influences during data capture. On the other hand, the yaw data from the integrated angular rate offers a steadier but gradually drifting picture due to its cumulative nature. The complementary filter's main application is to capitalize on the merits of both techniques, guaranteeing the best accuracy. As such, a high pass filter is applied to the integrated angular rate and a low pass filter to the magnetometer output. The outcomes are then combined to produce a reliable yaw angle estimate for the entire data span. The resulting yaw from our complementary filter aligns closely with the IMU-based yaw, with slight variations rooted in external disturbances affecting the magnetometer.

Velocity Estimation

With an accurate grasp on the vehicle's orientation, our next step was to gauge its velocity at each data point. We employed multiple techniques, leveraging both IMU and GPS

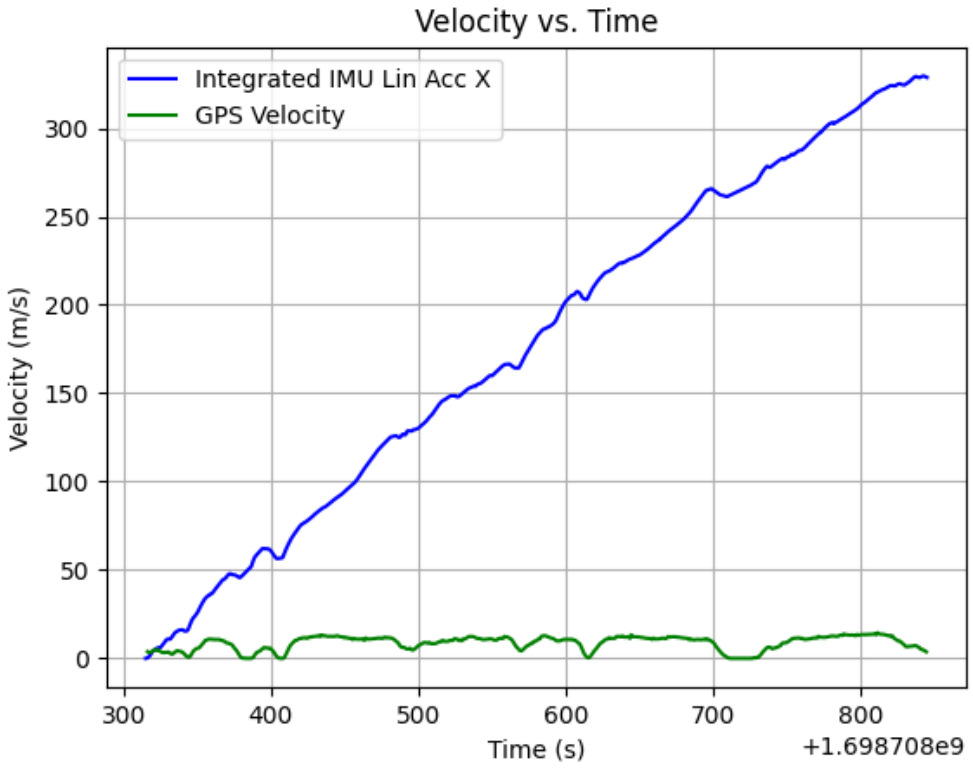

Figure 5

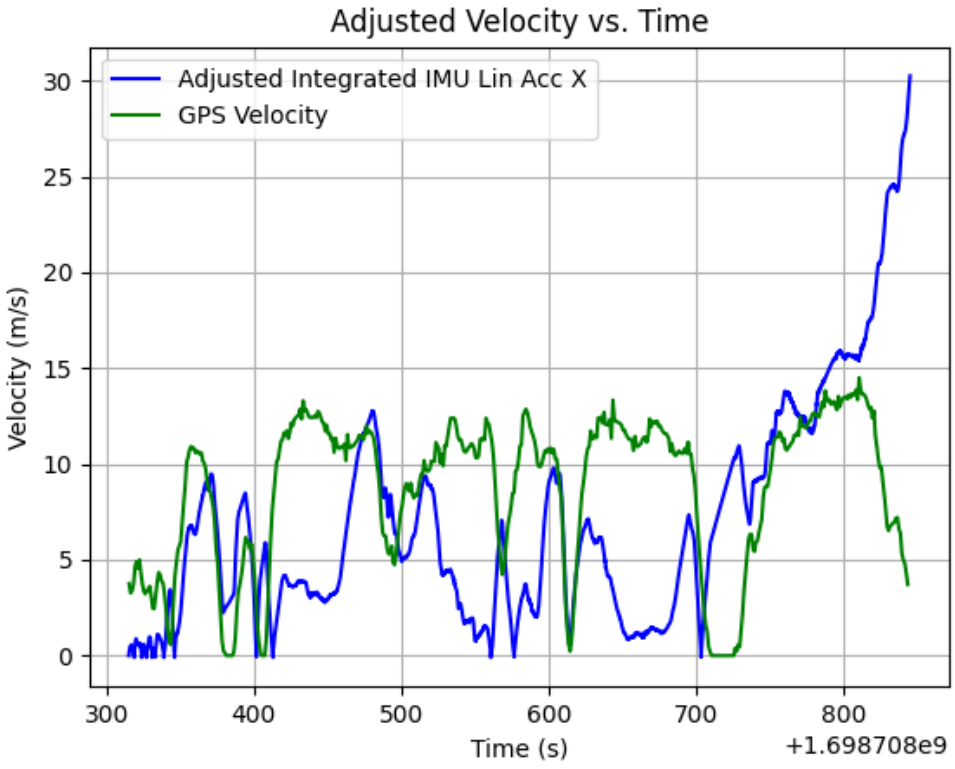

Figure 6

Upon analyzing the two figures, clear differences between the velocity plots emerge. Figure 4 reveals a divergence between the Integrated IMU Linear Acceleration and GPS Velocity. The GPS position's derivative estimation appears more consistent, mostly staying under 12 m/s and often returning to near 0 m/s, suggesting stationary moments like stops at traffic lights or congestion. In contrast, the integrated IMU acceleration indicates a continuous velocity increase, implying an implausible speed of 250 m/s.

Several factors contribute to this discrepancy: Accelerometer Bias: The accelerometer picks up gravitational forces. If the IMU isn't perfectly aligned during the drive, this unintentional acceleration is mistakenly added to the X-direction readings. Sensor Noise: Due to the accelerometer's high sensitivity, it can produce unstable readings even when stationary. To enhance the IMU acceleration data's precision, I applied a bias correction. I first determined the average bias from the stationary data at the start of the journey and then subtracted this from the X-direction acceleration measurements. After this correction, the integrated IMU data displayed a consistent drift that better matched the GPS position data.

These corrective measures, combined with the original IMU and GPS velocity data, are illustrated in Figure 5. As a result, the IMU-derived velocity data now more accurately reflects the GPS data, providing a truer depiction of the vehicle's speed progression.

Dead Reckoning:

Having obtained accurate estimations for both the vehicle's orientation and velocity throughout our journey, we can now infer its trajectory. It's essential to first juxtapose these findings with theoretical benchmarks. This will give us insights into potential discrepancies and their possible causes.

One key aspect we want to delve into is the relationship among the linear acceleration in the Y direction (denoted as Y" or Y double dot), the yaw rate around the Z axis (represented as Wz), and the velocity in the X direction (notated as X' or X dot). The interplay among these parameters can be encapsulated by the following equation:

$$Y_{double\ dot} = W_Z * X_{dot} \qquad \text{(Eq. 3)}$$

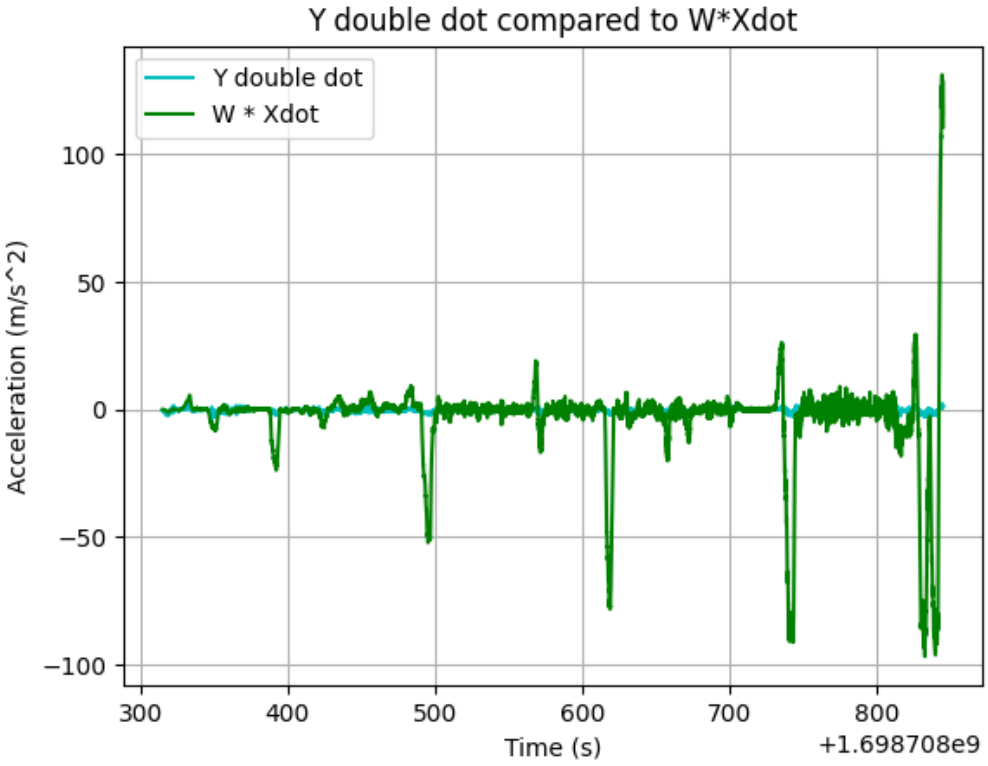

Figure 7

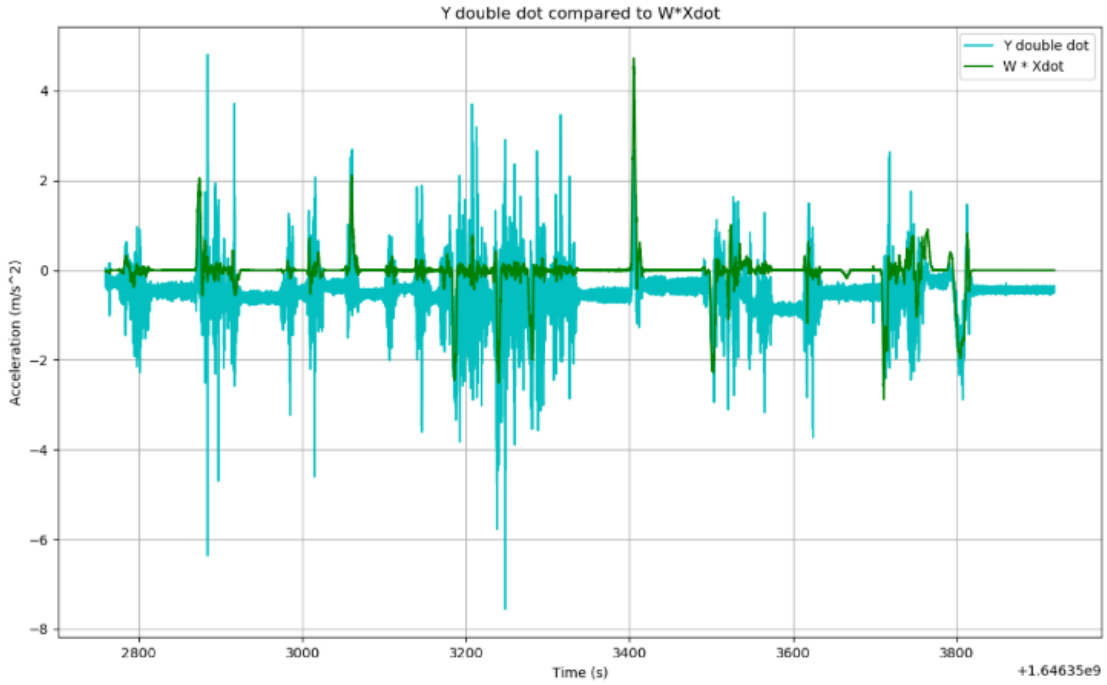

Figure 8

Both graphs closely align in their overall patterns. Specifically, spikes in the Y-direction linear acceleration (as captured by the IMU) coincide with spikes in the graph of the angular rate Z multiplied by X velocity. This alignment validates the relationship presented in Equation 3.

Differences Before Adjustment (Figure 7): The IMU's Y acceleration data shows a distinct bias. One major contributor to this is gravitational influence, which affects the Y-direction acceleration consistently. The integrated acceleration in the X direction (Xdot) presented here has been fine-tuned — it's stripped of the gravitational effect and aligned closer with GPS readings. As these Xdot values have undergone corrections for biases and noise reduction, they provide a more accurate representation than the raw IMU data, resulting in a cleaner presentation in Figure 7.

Differences After Adjustment (Figure 8): This illustration showcases the Xdot without interventions to negate static biases or eliminate noise. This direct representation clarifies the variations in bias between Figures 7 and 8. However, there remain inconsistencies between the two sets of data. These differences mainly arise from the noise in the integrated linear acceleration in the X direction. The combined effect of angular rate and Xdot is generally of a higher magnitude, amplifying potential inaccuracies compared to the singular Y-direction linear acceleration. When stationary, data oscillations occurred due to these biases, leading to inaccurate readings. The angular rate's product with Xdot tends to highlight these disparities more, particularly when compared to Y-direction linear acceleration.

In summary, while the initial data provides an unfiltered view, the adjusted data delivers a refined, clearer understanding of the vehicle's movements. This comparison emphasizes the critical role of data refinement in ensuring accuracy and reliability.

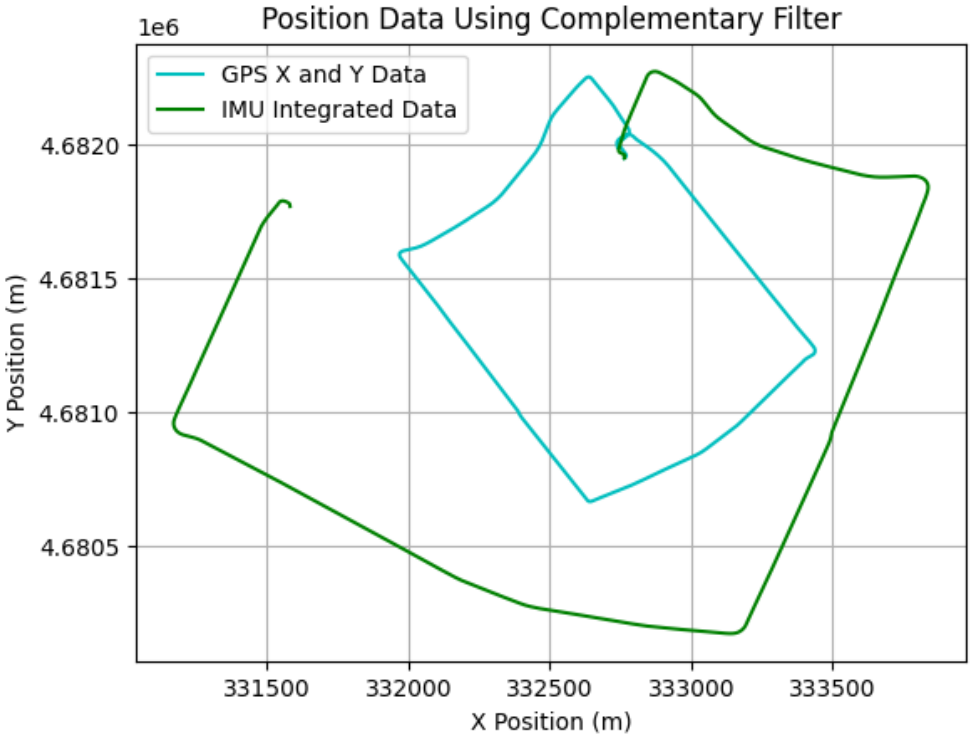

Figure 9

Comparison of Trajectories:GPS X and Y Data: This path, which forms a smaller loop, is the reference trajectory captured by the GPS. The continuity and relative compactness of this path suggest consistent and accurate tracking by the GPS.

IMU Integrated Data: The IMU data, forming a larger loop, represents the position data as calculated by integrating acceleration values from the IMU. There's an evident disparity between the GPS and IMU paths. The IMU track is more extended, which could imply that the IMU might be overestimating the traveled distance or direction changes at certain points.
IMU Loop Limitation:Despite the noticeable discrepancy, it's evident that there's a conscious effort to restrict the IMU data from forming a full loop. This could be a result of the application of a complementary filter or another correction technique. Such an approach ensures that IMU's inherent drift and cumulative errors don't cause a runaway trajectory. It's an acknowledgment of the sensor's limitations and an attempt to keep its data within a reasonable range of the GPS readings.

Sources of Discrepancy:IMU Drift: IMUs are notorious for their cumulative errors over time, primarily due to the drift. The integration of acceleration to obtain position can introduce small errors at each step, which, when accumulated, can lead to significant positional disparities.

GPS Accuracy: While GPS data is generally more stable over long durations compared to IMU, it's not entirely free from errors. Environmental factors like tall buildings or tree cover can affect the accuracy of GPS readings.Noise and Bias in IMU: The inherent noise in IMU readings and potential biases can cause discrepancies when data is integrated to derive position.

Benefits of Complementary Filter: The graph's title mentions the use of a complementary filter, a technique commonly employed to combine the strengths of two sensors (like GPS and IMU) to mitigate their individual weaknesses. This filter might be the reason the IMU path, though deviating, doesn't stray as far as one might expect without any correction. while the IMU provides high-frequency data and can track quick changes in direction or speed, its long-term accuracy is compromised due to inherent drift. On the other hand, the GPS provides stable long-term position data but might not capture quick, transient movements as effectively. The graph underscores the importance of combining data from both sensors to achieve a more accurate and reliable positioning system.

To deduce the location of the IMU device with respect to the vehicle frame, one needs to contemplate the kinematics. If we proceed with the assumption of no horizontal sliding in the Y direction, it means all velocities and accelerations in the Y direction are nullified. Under this premise, let's explore the relation further.

The center-of-mass (CM) of the vehicle is defined by its position, denoted as R, and its velocity, denoted as V. Contrary to placing the inertial sensor at the CM, it's located at a displacement, represented by a vector. This vector's x-component is the position we're trying to determine, termed as x_c, and it remains unchanged in the vehicle frame.
The vehicle's rotation is characterized by its rate, signified by a symbol ω. This denotes how fast the vehicle is rotating about its CM.

The speed of the sensor isn't solely dependent on the CM's velocity. It also has an added component because of the vehicle's rotation. To put it in mathematical terms, the velocity of the sensor is the sum of the velocity of the CM and the product of the rotation rate and the

displacement vector.

Expanding upon this, the acceleration of the inertial sensor can be seen as the rate of change of its speed. Using the derived relationships, we can express the sensor's acceleration as the sum of the CM's velocity, the product of the rotation rate and the displacement vector, and another term involving the product of the rotation rate and the previously mentioned sum. This framework is pivotal for computing x_c, the IMU's location concerning the vehicle frame. With the right data, we can manipulate this relationship to solve for x_c, offering an approximation of where the IMU device is positioned. Which lead Xc = -4.458719880832208 as result.

Conclusion

IMU and GPS are both potent technologies for positioning, each boasting its own set of strengths and limitations. This study clearly shows that GPS excels in tracking over extended distances and durations compared to IMUs. On the other hand, IMUs are particularly adept at precisely capturing minute alterations in a vehicle's orientation over longer time spans. Recognizing their respective strengths, along with understanding the impact of factors like noise, gravity, and external influences on the data, is vital for their optimal utilization in positioning tasks. When harmoniously combined, they furnish the essential tools to accurately determine the position and orientation for a myriad of robotic endeavors.

Questions answering

Calibration Procedure: The method utilizes magnetometer readings during vehicular circular motion, averaging these values to counteract persistent biases, termed as hard-iron correction. This correction is achieved by deducting the averaged values from the raw data. Magnetometer distortions generally emanate from two sources: hard-iron (constant biases) and soft-iron distortions (scaling and tilting effects).

Complementary Filter Usage: The yaw estimate derived from the integrated angular velocity is combined with the yaw estimate from the magnetometer using a complementary filter. The weighting given suggests a heavy reliance on the gyro data (90%) with a smaller influence (10%) from the magnetometer. Yet, there's no explicit mention of the cutoff frequency.

Reliability of Yaw Estimate: The yaw_filtered value from the complementary filter stands out as the most reliable for navigation. This is attributed to the filter's blending of the gyroscope's responsiveness with the magnetometer's long-term stability. The fusion offsets the inherent drift in gyroscopes and the magnetometer's susceptibility to external magnetic disruptions.

Acceleration Bias and Zero-Velocity Updates: I determined the accelerometer bias by computing the average of the stationary data from the initial 10 seconds. This bias was then subtracted from the moving accelerometer readings to offer a truer linear acceleration representation. Furthermore, to tackle drift in integrated velocity data, a threshold was applied, resetting the velocity whenever it dipped below this limit.

IMU vs. GPS Velocity Analysis: Figures 5 and 6 reveal marked disparities between velocities derived from the IMU and the GPS. While adjustments bridge this gap to some extent, discrepancies persist, largely from IMU drift and noise. Both techniques pose unique challenges, and adjustments, though helpful, don't achieve full congruence.

Trajectory Insights from Figure 9: This figure contrasts the vehicle's GPS-based trajectory with the path inferred from the IMU data. The GPS trajectory is smoother compared to the somewhat jagged path suggested by the IMU data. Introducing a complementary filter that amalgamates the two offers a balanced trajectory estimate, leveraging the strengths of both systems.

Analysis of w_xdot and Xc: The derived_wz variable emerges by relating angular velocities to time differentials. Data integrity checks flag zeros in derived_wz and NaN values. The final Xc value, representing the relationship between linear acceleration and derived angular velocity, emerges from a series of calculations. Xc, derived from vehicle motion data. Initially, w_xdot is formed by multiplying specific columns from the 'moving_imu' data, representing angular velocities and linear accelerations. The next step involves computing time differentials from consecutive time values of the 'moving_imu' dataset.

Subsequently, a variable called derived_wz is computed by dividing angular velocities by these time differentials. The data integrity is then ensured by checking for any zero values in derived_wz and potential NaN values in both arrays. If zeros are found in derived_wz, they are substituted with a very small non-zero number to avoid computational anomalies.

Finally, Xc_tot is calculated by taking the negative ratio of w_xdot to derived_wz. After filtering out any NaN values, the mean of Xc_tot gives the final value for Xc. This calculation appears to provide insights into the vehicle's motion characteristics by assessing how linear acceleration relates to the derived angular velocity.

VectorNav's Dead Reckoning Capabilities: Based on the presented trajectory graphs and the Xc value, the VectorNav showcases impressive dead-reckoning capabilities. The near-alignment of IMU and GPS data for most of the trajectory and the Xc value hint at consistent corrections during filtering, potentially compensating for IMU drift. To draw a definitive conclusion, comparisons with the manufacturer's specifications would be essential. The more close with the two lines for displacement with GPS and IMU will get better accuracy, the importance of position correcting become less. In my data shows reasonably good performance in dead reckoning, especially if the deviations are within the 2m range.